Journal of Nuclear Materials 561 (2022) 153568

Contents lists available at ScienceDirect

Journal of Nuclear Materials

journal homepage: www.elsevier.com/locate/jnucmat

High-temperature compressive creep tests of U_3Si_2 with spark plasma sintering: Experiments and finite element modeling

Bowen Gong[a], Dong Zhao[a], Andre Broussard[a], Jason Harp[b], Andrew T. Nelson[b], Jie Lian[a,c,*]

[a] Department of Mechanical, Aerospace and Nuclear Engineering, Rensselaer Polytechnic Institute, United States
[b] Oak Ridge National Laboratory, Oak Ridge, TN 37830, United States
[c] Department of Materials Science & Engineering, Rensselaer Polytechnic Institute, United States

ARTICLE INFO

Article history:
Received 8 December 2021
Revised 24 January 2022
Accepted 26 January 2022
Available online 29 January 2022

Keywords:
SPS
High-temperature creep testing
Nuclear fuels
Finite element modeling

ABSTRACT

This paper reports a systematic high-temperature creep behavior of dense U_3Si_2 pellets using a spark plasma sintering (SPS) apparatus at elevated temperatures and pressures under vacuum conditions. The stress exponent was subsequently derived to be 3.21 at 1173 K and 2.17 at 1223 K, respectively, indicating a grain boundary sliding creep mechanism. The creep activation energy was determined to be 203.6 ± 19.0 kJ/mol, which agrees well with the literature. Finite element modeling was performed using the creep parameters fitted from the strain-time plot. The results suggest an excellent match with the experimental data, confirming the validity of the experiments. Microstructure characterizations indicate that the main phase of the specimens after creep tests remains to be U_3Si_2, with a 4 μm thick layer of nano-sized particles induced from the diffusion between U_3Si_2 and alumina disc used to avoid electric current passing through the sample. The successful conduct of creep experiments demonstrates the great potential of SPS to perform high-temperature mechanical testing of nuclear fuels under vacuum conditions. The subsequent finite element modeling exhibits excellent capabilities for accurately predicting material performance in the creep tests and provides a practical tool in evaluating nuclear fuels' performance for a much-extended time scale.

1. Introduction

U_3Si_2, as a potential candidate of accident tolerant fuels (ATFs), has drawn attention ever since the Fukushima accident. Extensive research has been focused on the development of advanced fuels that display enhanced performance and improved safety margins. U_3Si_2 has a significantly higher uranium loading than UO_2 [1] and exhibits a much improved thermal conductivity that increases with temperature [2–4]. The increasing thermal conductivity leads to reduced stored energy and better heat removal efficiency, especially at elevated temperatures, which helps to reduce the risk of melting or other failure modes under extreme conditions. During reactor operation, nuclear pellets typically experience high temperature, high pressure, and steam corrosion. Modified U_3Si_2 fuels can be designed to tune their resistances to oxidation and steam corrosion. In a recent study regarding oxidation resistance of monolithic U_3Si_2, we reported improved onset temperatures for both SPS-densified microcrystalline (793 K) and nanocrystalline specimens (783 K), higher than that of UO_2 [5] and U_3Si_2 prepared with arc melting [6]. A strain effect is attributed to the improved oxidation resistance of U_3Si_2 fuels, which can be introduced from the SPS process. In a study about the steam resistance of U_3Si_2 [7], we reported that U_3Si_2 has a poor performance in steam, displaying rapid loss of mass from around 732 K and loss of structural integrity in the isothermal steam testing at 623 K. However, after Cr doping, the U_3Si_2 specimens exhibit outstanding steam corrosion resistance, both in ramping test and isothermal test [8]. Both 5 wt% Cr-doped U_3Si_2 and 10 wt% Cr-doped U_3Si_2 specimens remain their original weight until ~793 K. The 10 wt% Cr-doped pellet remains its integrity in the isothermal steam test under 633 K for at least 24 hours. These findings indicate that Cr doping can indeed improve the corrosion resistance of materials. In addition to Cr [9], other additives-incorporated U_3Si_2 such as Al [9,10], Y [9], and 3Y-TZP [11] were also extensively studied. Composite fuels by combining silicides with other leading fuel concepts were also studied to combine their merits together to improve fuel performance. For example, Gong et al. [12] fabricated UN+UO_2 composites with onset temperatures for oxidation above 773 K and simultaneously enhanced fracture toughness and thermal conductivity. U_3Si_2/UN composites were also fabricated by White et al. [13] though with inferior performance due to

* Corresponding author at: Department of Mechanical, Aerospace and Nuclear Engineering, Rensselaer Polytechnic Institute, United States.
E-mail address: lianj@rpi.edu (J. Lian).

https://doi.org/10.1016/j.jnucmat.2022.153568
0022-3115/

micro-cracking induced from the thermal mismatch between UN and U_3Si_2. By controlling SPS sintering conditions and cooling parameters, the micro-cracks in the U_3Si_2/UN can be mitigated with improved thermal-mechanical properties and oxidation resistance [14].

Mechanical properties, including hardness [8,12,15–18] and Young's modulus [18–20], are also of great significance and interest for nuclear fuels and have been extensively investigated for U_3Si_2 fuels. Among all of these properties, the high temperature creep behavior of nuclear fuels is a key fuel property profoundly impacting the fuel cladding mechanical interaction, and the fuel matrices are applied with high compressive stress from the cladding at elevated temperatures. Generally, the creep process can be categorized into three stages including primary, secondary, and tertiary phases. The primary stage was a result of hardening from the substructure development [21], which features an increase in strain with a decreasing strain rate. The secondary phase witnesses a constant (steady-state) strain rate, critical for the longevity of the component under applied stress, and the tertiary phase displays a much higher strain rate (force-controlled loading). Different stages of the creep curve are the outcome of microstructural change and the competition between two contrary processes, i.e., hardening and recovery [22]. Hardening increases the strength of the material through the dislocation movement and generation, while recovery removes these accumulated defects and promotes further deformation.

However, it is difficult to perform high temperature creep measurements of nuclear fuels, particularly for silicides, nitrides, and metallic fuels, which are highly sensitive to oxidation at elevated temperatures. High temperature creep testing should be performed in a controlled environment with well-controlled oxygen exposure, and the creep test involves the long-term application of stress. Therefore, high-temperature creep data for nuclear fuels are scarce in the literature due to constraints for high temperature creep testing that requires long-term operation under both high temperature and high pressure in an oxygen-controlled environment. Limited data on UO_2 fuels were reported in the literature. Frazer et al. [23] used a MicroMaterials Platform indenter to perform the creep test on UO_2 up to 773 K and derived the stress exponent for SPS-sintered and conventional UO_2 pellets. However, the total running time was 5 min due to the limit of the apparatus. The creep behavior of stoichiometric UO_2 was investigated with a bending apparatus in the temperature range of 1523–1673 K with a pressure of 700 to 16,000 psi. The activation energy was measured to be 91 $\pm$ 8 kcal [24]. The creep activation energy of single-crystal UO_2 during the first stage of the creep was derived to be 5.1 eV with four-point loading testing at a temperature range of 1613–1958 K and a stress range of 3600–8000 psi. Recently, Mercado [25] performed creep testing of multiple U_3Si_2 samples for much extended period, up to 900 h. The authors tested U_3Si_2 samples under different combinations of temperature and pressure and derived an activation energy of 168 kJ/mol. Metzger [26] developed models for simulating creep behavior of U_3Si_2 and stated that when temperature is 873 K and stress is above $G \times 10^{-4}$ (G is the shear modulus), the creep mechanism is likely to be dominated by the dislocation creep mechanism.

In the current work, we report the high-temperature creep tests of U_3Si_2 using spark plasma sintering with controlled temperature and pressure in a vacuum environment. The relationships between strain vs. time and strain rate vs. strain were examined, indicating a primary creep stage. Stress exponents at different temperatures were derived to be 3.21 at 1173 K and 2.17 at 1223 K, suggesting a dominant creep mechanism of grain boundary sliding. The apparent activation energy was calculated from the Arrhenius equation to be 203.6 $\pm$ 19 kJ/mol, which matches with the literature. Finite element modeling on the creep behavior of the specimens was further performed with the same geometry as the testing specimen and the derived creep parameters. The results agree well with the experiments, suggesting that the finite element models can be used to accurately simulate the creep experiments, and therefore, can be utilized to estimate the strain and stress response of specimens for a much-extended time. Microstructure characterization on the specimens after creep tests suggests that the samples retain their integrity and phase with no oxidation after 8 hours of high-temperature tests. These results demonstrate that SPS, commonly used as an advanced fuel fabrication technology, holds immense potential to be used as a unique high-temperature mechanical property testing apparatus for nuclear fuels, which are typically difficult to be measured. The combination of experiments and finite element modeling makes it possible to predict the creep behavior of nuclear fuels at longer timescales, which greatly enhances our capability of evaluating nuclear fuel performance under extreme conditions.

2. Experimental details

2.1. Densification of U3Si2 by SPS for high temperature creep testing

The U_3Si_2 powders used for dense fuel pellet fabrication were manufactured by Idaho National Laboratory (INL) through powder metallurgy, involving a series of operations such as powder mixing of uranium and silicon, multi-current arc melting, and high-temperature thermal annealing. The detailed manufacturing procedures were described earlier in [27]. The U_3Si_2 powders were ball milled with a high-energy ball milling (HEBM) to reduce the particle size before sintering [16,28]. The ball milling apparatus used is a Pulverisette 7 planetary micro mill (Idar-Oberstein, Germany). One ball milling cycle typically consists of 15 min running time and 10 min idle time, with a rotating speed of 500 rounds per minute. 4-cycles were run for each batch of powders. All of the powder preparation operations were handled in a glovebox with an oxygen level lower than 1 ppm. Before the sintering, $\sim$ 3.5 grams of U_3Si_2 powders were loaded into a graphite die, wrapped by a thin graphite foil. Two pieces of graphite discs were placed at two sides of the powder compact to separate the powders and the graphite punch. The graphite die was wrapped by a piece of graphite felt to reduce heat loss during the sintering, and then the whole assembly was placed into the chamber of the SPS apparatus (Thermal Tech, SPS 10–3, Santa Rosa, California). During the sintering, the temperature was measured by a thermocouple. Temperature ramps from room temperature to 1323 K with a heating rate of 100 K/min, then the specimen was isothermally held for 5 mins with the pressure ramping from 15 MPa to 50 MPa. After sintering, the pressure was immediately released to allow for free cooling of fuel pellets. The sintered fuel pellets were ground to remove the graphite foil and polished with silicon carbide papers. The physical density was measured with an Archimedes method. The sintered pellets have a height of $\sim$5 mm and a diameter of $\sim$8 mm.

2.2. High temperature creep testing on U3Si2 pellets by SPS

The polished U_3Si_2 specimen was placed into the chamber of a graphite die, which has a diameter of 25 mm. At one side, a thin alumina disc was placed between the graphite punch and the sample to avoid the electric current passing through the specimen since it was reported that electric current would have an impact on the creep behavior of the test specimens [29]. The disc has a diameter of 25 mm and a thickness of 0.65 mm. On the other side, two graphite discs with both sides sprayed with boron nitride were placed on the sample instead of an alumina disc to avoid possible effects from the crack of the alumina disc. The whole graphite die

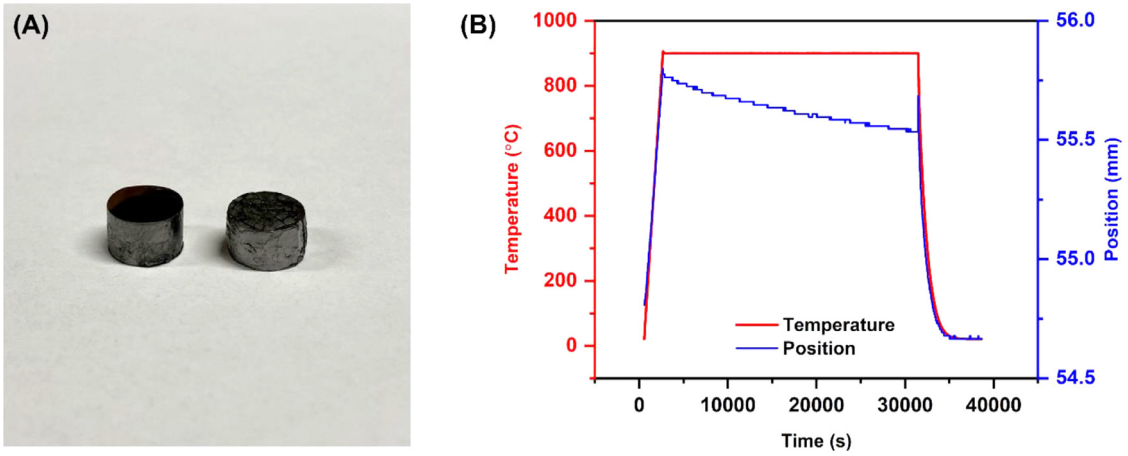

Fig. 1. (A) U_3Si_2 pellets prior and after high temperature creep tests, and (B) A representative plot of recorded temperature and displacement during the creep test of U_3Si_2 pellets for 8 h.

was wrapped with two layers of graphite felt, including the top of the die to avoid any heat loss. A thermocouple was inserted into a small hole on the wall of the die and stayed in contact with the sample to measure its surface temperature during the whole testing. The chamber keeps a vacuum of lower than 2×10^{-2} torr during the testing to avoid any oxidation to the specimen. Before the sample heats up, a pressure of 15 MPa was applied to the sample. After the beginning of the creep testing, the pressure increases from 15 MPa to the testing pressure with a rate of 5 MPa/min, then temperature increases from room temperature to the testing temperature with a rate of 25 K/min. The temperature was held at the testing temperature for the following 8 hours before the program terminated. After the test, the specimens were taken out, and the top and bottom surfaces were polished for microstructure characterization. In the current work, two temperatures and two stresses were considered, where the testing temperatures were above the threshold of the thermal creep regime, which is around 0.45 T_{melt} (melting temperature) [30]. For U_3Si_2, its melting point T_{melt} is 1938 K [31], thus requiring the creep testing temperature to be above 1023 K. These temperatures are also representative of the calculated centerline temperatures within the range of 973–1273 K for U_3Si_2 if used as an LWR fuel [32–34]. For testing pressure, the creep tests were conducted at 60 MPa and 70 MPa, which is above the sintering pressure and approaches the stress limit of the graphite punch used.

2.3. Microstructure characterization of sintered specimens and after creep testing

The microstructure of the sintered specimens and samples after creep testing were characterized by a field-emission scanning electron microscopy (SEM, FEI Versa 3D, Oregon, US). X-ray diffraction (XRD) patterns of each specimen were obtained through a Panalytical X'Pert XRD system (Westborough, MA, USA) with Cu Ka irradiation, the wavelength of which is 1.5406 Å. The scanning range is 20°–80°, and the scanning step is 0.05° with a scanning rate of 2 s/step.

2.4. Finite element modeling

Finite element models were created in Abaqus®, with the same dimensions as the actual testing specimens. The material properties of the models were then specified. Specifically, Young's modulus was 130 GPa [19], and Poisson's ratio was 0.2 [35]. The coefficient of thermal expansion was 16.1×10^{-6} K^{-1}. The creep models commonly used in Abaqus are the time-hardening model and the strain-hardening model, both of which were based on the power-law creep model. Under certain circumstances and constraints, these two forms of hardening can be unified [36]. In the current modeling, time-hardening was used for its simplicity. Three parameters were specified, including power law multiplier A, stress order n, and time order m based on the time-hardening model shown below in Eq. (1) [36], where $\dot{\epsilon}$ is the creep strain rate, q is the stress, and t is the creep time. Integrating Eq. (1) leads to Eq. (2), where ε is the strain. The input values of A, n, and m were obtained by fitting the strain-time curve obtained from each specimen. The creep behavior was modeled via the Visco step, which depicts the time-dependent response for transient stress-displacement analysis and is commonly used to model the creep behavior in Abaqus [37]. The time for this step was specified as 28,800 s, corresponding to 8 h, which is the same as the experiment. The minimum time increment is 0.288, and the creep strain error tolerance was set to 0.1. The temperature of the model was specified through the predefined fields from the initial step. The load was applied through evenly distributed pressure to the top surface, while a *ZSYMM* boundary condition was specified for the bottom surface of the sample such that there is symmetry about plane z. For the mesh, the approximate global size was 0.2 mm, the element shape was Hex, with a sweep meshing technique. The element type was 3D stress with linear geometric order.

$$\dot{\epsilon} = Aq^n t^m \tag{1}$$

$$\epsilon = \frac{A}{1+m} q^n t^{m+1} \tag{2}$$

3. Results and discussion

3.1. Creep behavior of U_3Si_2 evaluated with SPS

Fig. 1A shows the SPS-sintered U_3Si_2 specimens before and after the creep test, the diameter of the specimen is ~8 mm, and the thickness is around 5.5 mm. Both surfaces were fine-polished to ensure their parallelism. Noticeable deformation can be observed for all U_3Si_2 specimens after creep testing at high temperatures and pressures. The deformed specimen after the test obviously shows that the deformed pellet geometry is shortened in thickness and increased in diameter. Unlike other creep studies with SPS [38], in this study, constant stress was applied to the specimen such that the true stress remains constant during the test instead of decreasing due to the increase in the cross-section. Fig. 1B shows a representative plot of temperature and position of the piston vs. time during the test. It can be noticed that with the in-

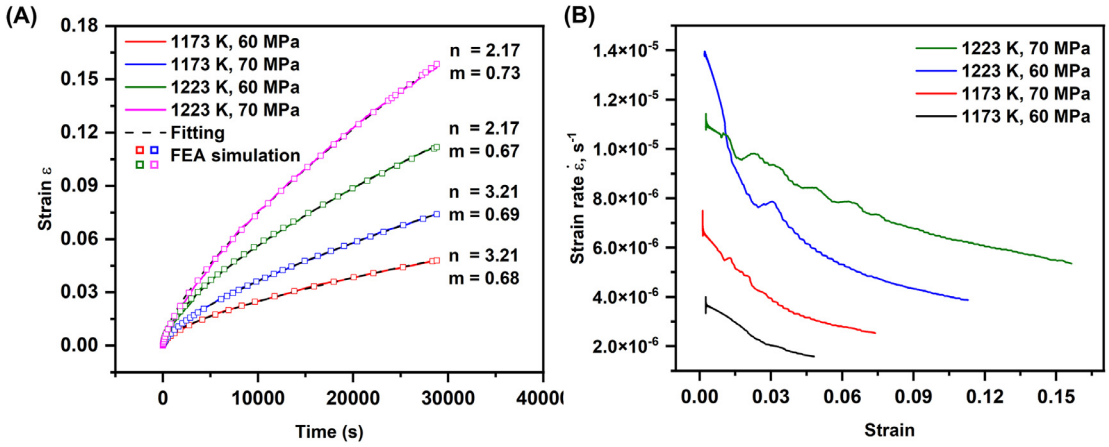

Fig. 2. (A) The plot of strain vs. time at different temperatures and pressures, along with the fitted data and finite element modeling results. The derived key creep parameters, such as stress exponent n and time exponent m, are marked aside of each curve. Higher temperature and higher pressure lead to higher strain at all times; (B) The plot of strain rate and strain showing a monotonic decrease due to work hardening, suggesting a primary creep stage. Higher temperature and higher pressure result in higher strain rates.

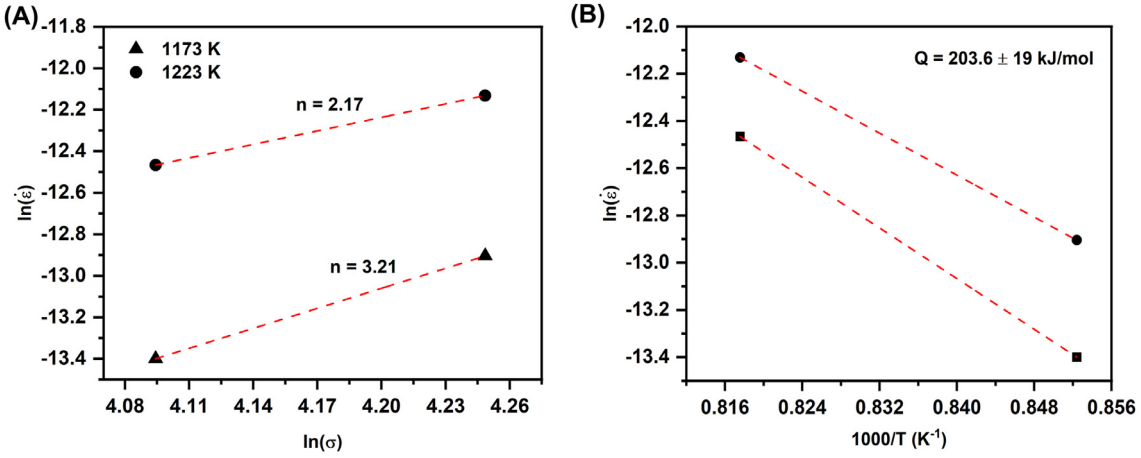

Fig. 3. (A) The plot of logarithmic strain rate vs. logarithmic stress. The stress exponent was derived to be 3.21 at 1173 K and 2.17 at 1223 K, suggesting that the creep mechanism is grain boundary sliding; (B) an Arrhenius plot to determine the activation energy of U_3Si_2 upon high temperature creep testing.

crease of temperature, the recorded position increases first until the testing temperature is reached. This is mostly due to the thermal expansion of the graphite spacer. Subsequently, the position starts to decrease gradually until the end of the test.

The strain was calculated based on Eq. (3) below, where Δl represents the specimen length change, and l_0 is the initial sample thickness. All strains indicated are nominal values referring to the dimension of the original sample. All stresses indicated are true stress since the testing process is stress-controlled instead of force-controlled.

$$\epsilon = \frac{\Delta l}{l_0} \tag{3}$$

The solid lines in Fig. 2A show the plot of strain vs. time obtained from the experiments at various temperatures and pressures. The strain data were smoothed with a window size of ~1000 to ensure the correct calculation of strain rate. Several observations can be made from Fig. 2A. Firstly, all of the creep curves increase with time, suggesting that the specimens experience continuous thickness shrinkage. Secondly, when the temperature increases or stress increases, a higher strain can be expected as materials become more ductile at higher temperatures. Generally, the creep process can be divided into three steps, i.e., primary, secondary, and tertiary creep. For the creep with a constant load and constant stress, the first two steps in the strain-time plot are generally overlapped. The distinction of these two loading methods starts from the tertiary step, where strain rate increases fast for constant-load creep, while keeping a constant value for constant-stress creep. All specimens tested under various temperatures and pressures are in the primary stage of the creep within the first 8 hours. Work hardening [39] can be observed in all samples, which decelerates the strain rate. As indicated in [38,39], a quasi-steady-state can be defined if the strain rate tends to approach a limit, which corresponds to the quasi-steady-state strain rate. Fig. 2B shows the plot of strain rate vs. strain for all specimens. The strain rate was calculated as the derivative of the strain curve based on the normal strain based on original dimensions. The plot shows that strain rate decreases as strain increases, suggesting work hardening in all specimens.

An Arrhenius equation shown in Eq. (4) is commonly used to depict the relationship between strain rate, stress, temperature, and creep activation energy, specifically for the secondary creep or quasi-steady-state reported in the current work, where $\dot{\epsilon}$ is strain rate, A is a pre-exponential factor, n is stress exponent, T is the temperature in unit K, R is gas constant, and Q is the activation energy for creep. When the temperature remains the same, the last term can be regarded as constant, and Eq. (4) can be further simplified to Eq. (5), where strain rate is only a function of stress. Taking the logarithm at both sides, Eq. (6) can be obtained. By plotting logarithmic strain rate and logarithmic stress, the stress

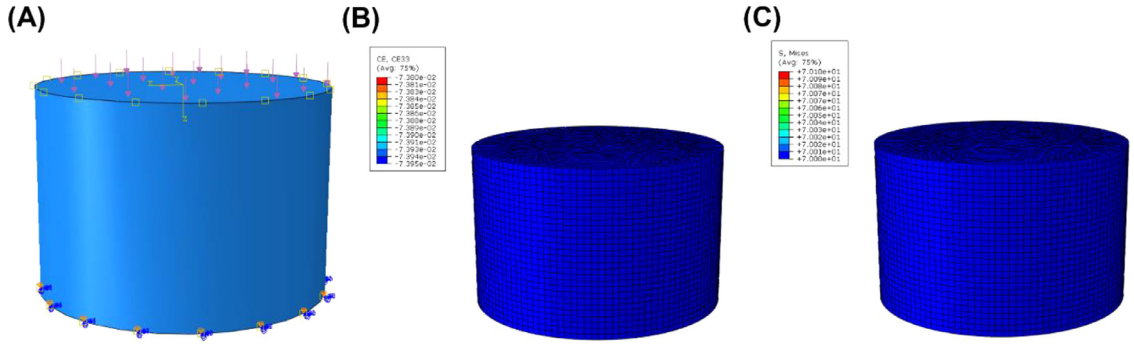

Fig. 4. Finite element models for the specimen tested at 1173 K and 70 MPa: (A) load and boundary during the test, (B) uniaxial strain at the end of testing, and (C) Von Mises stress in the specimen. Strain and stress can be seen to be uniformly distributed in the whole model.

exponent n can be derived. Fig. 3A shows the derived value of n, which is 3.21 at 1173 K, and 2.17 for 1223 K. It is common that n varies at different temperatures, which was reported in the literature [40–42] and may be due to a change of creep mechanisms at different temperatures. Based on the literature [21,43], creep with a stress exponent of 2 represents a creep mechanism due to grain boundary sliding accommodated by the formation of grain boundary cavities, while an exponent of 3.5 represents grain boundary sliding accommodated by triple point fold formation. After the derivation of n, Eq. (4) can be simplified as Eq. (7), since σ^n can be regarded as a constant now. Taking the logarithm at both sides, Eq. (8) can be obtained. The activation energy for creep can be further derived by plotting $\log\dot{\epsilon}$ and $1/T$. Fig. 3B shows the derivation of Q, which equals 203.6 ± 19.0 kJ/mol. Yingling [44] derived the activation energy for U_3Si_2 using different creep models. Specifically, using a power law as Eq. (4), activation energy was obtained to be 218.6 kJ/mol. If using an improved power law as shown in Eq. (9), the activation energy was 225.3 kJ/mol. Another two commonly used creep models are the Coble creep model and the Nabarro-Herring model, both of which are controlled by diffusion. Using the Coble creep model as shown in Eq. (10) (d is the average grain size), the authors obtained an activation energy of 208.7 kJ/mol. Lastly, with the Nabarro-herring method [45], activation energy was derived to be 173.4 kJ/mol. It can be seen that the experimentally derived activation energy for U_3Si_2 in this study matches pretty well with the simulation conducted by Yingling based on BISON [44], which is a finite element code for nuclear simulation. Mercado [25] derived the high-temperature activation energy of U_3Si_2 to be 168 kJ/mol with an exponent of 1.94, which is slightly lower than the value reported here and might be due to different sample geometry, microstructure, density, etc. In a recent paper by Yingling et al. [46] with updated U_3Si_2 thermal creep, the authors reported an activation energy of 223.1 kJ/mol with an exponent of 1.936 for the secondary creep stage, in line with the values achieved here.

$$\dot{\epsilon} = A\sigma^n \exp\left(-\frac{Q}{RT}\right) \tag{4}$$

$$\dot{\epsilon} = A\sigma^n \tag{5}$$

$$\log\dot{\epsilon} = \log A + n\log\sigma \tag{6}$$

$$\dot{\epsilon} = Bexp\left(-\frac{Q}{RT}\right) \tag{7}$$

$$\log\dot{\epsilon} = \log B - \frac{Q}{RT} \tag{8}$$

$$\dot{\epsilon} = \frac{A}{T}\sigma^n \exp -\frac{Q}{RT} \tag{9}$$

Table 1
stress and time exponent derived at different creep temperature and pressure.

Sample #	Testing temperature (K)	Testing Pressure (MPa)	n	m
1	1173	60	3.21	0.68
2	1173	70	3.21	0.69
3	1223	60	2.17	0.67
4	1223	70	2.17	0.73

$$\dot{\epsilon} = \frac{A\sigma}{Td^3} \exp -\frac{Q}{RT} \tag{10}$$

For creep strain in the primary creep stage, it can be characterized by the power law shown in formula (11) below [47], where ϵ_0 is the initial strain, m is the time exponent, and the other parameters have the same meaning as above. Note that a similar formula was used in Abaqus to describe the relationship among strain rate, stress, and time. After fitting the strain-time data obtained from the high temperature creep testing by SPS and the value of n obtained previously, the time component, m, can be derived and is shown in Table 1. No obvious trend was found for the time exponent m in this temperature range.

$$\epsilon = \epsilon_0 + A\sigma^n t^m \tag{11}$$

3.2. Finite element modeling of creep behavior of U_3Si_2

A representative finite element model for the U_3Si_2 specimen used in the creep testing is shown in Fig. 4A, where the bottom was constrained with Z-symmetry, and the top surface was applied with constant pressure. Fig. 4B and C show the contour plots of the strain on the uniaxial direction and the Von Mises stress on the deformed model after 8 hours of creep under 1173 K and 70 MPa. The color bar indicates that the strain and Von Mises stress are uniform for all locations in the model, and the variation is negligible. The variation of strain vs. time for all samples was plotted with scattered squares in Fig. 2A, which overlapped with the experimental data. This suggests that finite element models can be used to accurately simulate the creep experiments. Therefore, these finite element models can be utilized to further estimate the strain and stress response of specimens for a much longer time under constant stresses and thus are very useful to have a better understanding of the creep behavior of U_3Si_2 beyond the limit of experiments.

3.3. Microstructure characterization of U_3Si_2 specimens prior and after creep tests

Fig. 5A and B show XRD patterns for U_3Si_2 specimens that underwent creep tests at 1223 K, 70 MPa and 1173 K, 60 MPa. Specifi-

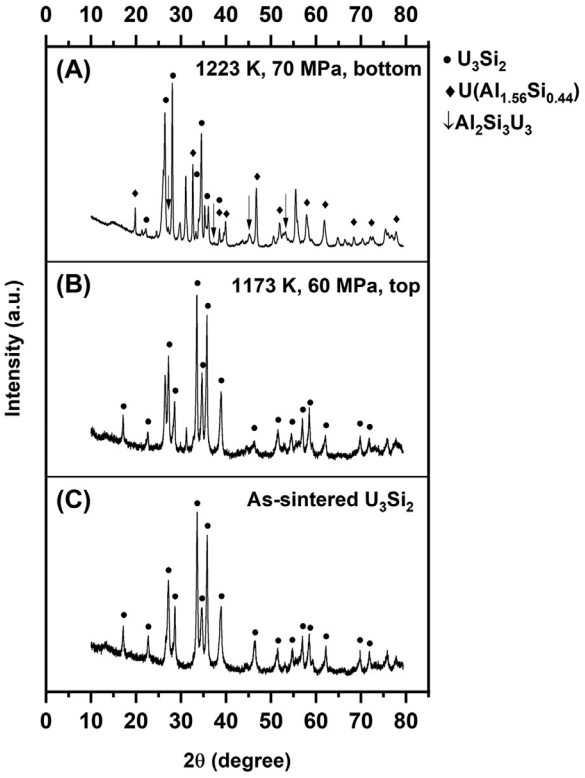

Fig. 5. XRD patterns of the U_3Si_2 specimens prior and after creep tests. The bottom surface of the specimen contacting with an alumina disc (A) showing the formation of U-Al-Si ternary phases; while the top surface of the specimen contacting with a boron nitride sprayed graphite disc (B) showing no oxidation or phase changes, compared to the as-sintered monolithic U_3Si_2 (C).

cally, the XRD pattern shown in Fig. 5A was acquired from the bottom surface of the sample in contact with the alumina disc, while the XRD pattern shown in Fig. 5B was acquired from the top surface of the sample in contact with the graphite foil sprayed with boron nitride. Fig. 5C shows the XRD pattern for the as-sintered sample, where all peaks can be indexed to monolithic U_3Si_2. It can be seen that for the top surface of the sample after the creep test, all peaks can still be indexed to U_3Si_2. No oxidation can be observed, suggesting that the samples still retain their original phase during the whole testing period. On the bottom surface in contact with the alumina disc, the majority of the peaks can still be indexed to U_3Si_2, but there are some other peaks that appeared as well, which can be indexed to $U(Al_{1.56}Si_{0.44})$ (PDF 01-071-4041) [6]. Minor peaks marked with downward arrows can be indexed to $Al_2Si_3U_3$ (PDF 00-048-1664) [6]. The appearance of U-Si-Al ternary phases suggests that during the high-temperature and pressure conditions, diffusion happens between the alumina disc and U_3Si_2. However, this does not impact the derivation of the activation energy reported above since even at 1223 K, 60 MPa for 8 hours, only a minimum diffusion layer was observed, with a thickness of less than 4 μm.

Fig. 6 displays a series of SEM images prior to and after creep tests. Fig. 6A shows the as-sintered U_3Si_2 specimen. It can be seen that the monolithic U_3Si_2 pellet is very dense and displays a uniform microstructure without secondary phases or obvious pores. Fig. 6B shows the top surface of the sample after the creep test at 1173 K and 60 MPa. Although the sample underwent the creep test for 8 hours, no obvious changes can be noticed in the sample. Fig. 6C shows the bottom surface of the sample after the creep test at 1173 K and 70 MPa, from which it can be seen that some cracks and bulges appeared. These features might be attributed to the formation of the U-Si-Al ternary phase because of the inter-diffusion between the fuel matrix and the alumina disc. Fig. 6D and E show enlarged views of the bulge that appeared at the bottom surface of the sample after the creep test at 1223 K and 60 MPa. It can be found that at both sides of the bulge, many nano-sized particles formed, which were believed to be the nano-sized particles of the ternary phase. Fig. 6E shows that the thickness of the layer with nano-sized particles is around 3.7 μm, below which the U_3Si_2 still retains its original microstructure. Fig. 6F shows the bottom surface of the sample after the creep test at 1223 K and 70 MPa after the removal of the ternary phase layer via grinding. Some pores and cavities can be seen from the SEM image, confirming that the creep mechanism at 1223 K is grain boundary sliding accommodated by the formation of grain boundary cavities.

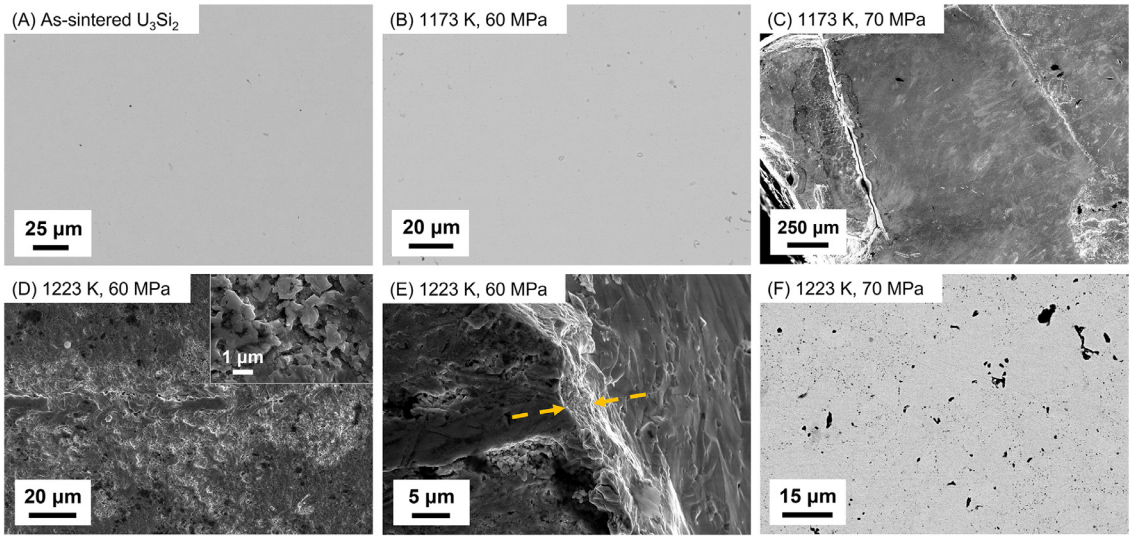

Fig. 6. SEM images of the U_3Si_2 specimens prior to and after the creep tests: (A) the surface of the as-sintered specimen shows the monolithic U_3Si_2 pellets are dense and display uniform microstructure and phases; (B) the top surface of the U_3Si_2 specimen after testing at 1173 K and 60 MPa, showing no obvious microstructural variation; (C) the bottom surface of the U_3Si_2 specimen tested at 1173 K and 70 MPa contacting with alumina disc, showing cracks due to the formation of U-Al-Si ternary phases; (D,E) the layer (thickness of ~4 μm) of the ternary phases featuring nano-sized particles; and (F) Vacancies on the grain boundaries of the polished bottom surface of the U_3Si_2 specimen tested at 1223 K and 70 MPa.

4. Conclusions

In summary, high-temperature compressive creep tests were successfully conducted on U_3Si_2 fuels using SPS in the temperature range of 1173–1223 K and the pressure range of 60–70 MPa. Temperature, pressure, and displacement of sample geometry were recorded *in-situ* during the tests, and the strain was determined. The strain was found to increase with time in all tests. The strain rate was calculated, and a monotonic decreasing trend was observed within the primary stage of the creep. The stress exponent was derived to be 3.21 at 1173 K and 2.17 at 1223 K based on the quasi-steady state, respectively, suggesting a grain boundary sliding creep mechanism. The activation energy was calculated to be 203.6 ± 19.0 kJ/mol, in excellent agreement with the literature. Finite element modeling with the time-hardening version of the power law model was used to simulate the creep behavior of the specimens. The results agree with the experiments, suggesting that these models can be used to accurately simulate the creep experiments, and therefore, can be utilized to estimate the strain and stress response of specimens for a much-extended time. Microstructure characterizations suggest that the sample remains as U_3Si_2 after the creep, and an inter-diffusion occurred between the fuel matrix and the alumina disc, leading to the formation of ternary phases with nano-sized particles. Cavities can also be observed at grain boundaries, confirming the grain boundary cavities creep mechanism. The systematic study of the creep behavior of U_3Si_2 with SPS demonstrates the great potential of using SPS as a unique approach for high-temperature creep testing of nuclear fuels with programmable temperature and pressure under minimum oxidation. The creep mechanisms and key parameters (such as the activation energy and the stress component) will be valuable to develop thermal creep models that can be used for predicting the performance of the nuclear fuels based on finite element modeling or engineering-based fuel performance codes.

Data availability

The data that support the findings of this study are available from the corresponding author upon reasonable request.

Declaration of Competing Interest

The authors declare that they have no known competing financial interests or personal relationships that could have appeared to influence the work reported in this paper.

CRediT authorship contribution statement

Bowen Gong: Conceptualization, Investigation, Methodology, Visualization, Writing – original draft, Writing – review & editing. **Dong Zhao:** Investigation, Visualization, Writing – review & editing. **Andre Broussard:** Investigation, Visualization, Writing – review & editing. **Jason Harp:** Resources, Writing – review & editing. **Andrew T. Nelson:** Resources, Writing – review & editing. **Jie Lian:** Conceptualization, Funding acquisition, Resources, Writing – review & editing.

Acknowledgment

This work was supported by the US Department of Energy's (DOE's) Office of Nuclear Energy under Nuclear Energy University Programs (award numbers: DE-NE0008532).

References

[1] D.A. Lopes, S. Uygur, K. Johnson, Degradation of UN and UN–U_3Si_2 pellets in steam environment, J. Nucl. Sci. Technol. 54 (4) (2017) 405–413.
[2] B. Gong, T. Yao, P. Lei, J. Harp, A.T. Nelson, J. Lian, Spark plasma sintering (SPS) densified U_3Si_2 pellets: microstructure control and enhanced mechanical and oxidation properties, J. Alloy. Compd. 825 (2020) 154022.
[3] J.T. White, A.T. Nelson, J.T. Dunwoody, D.D. Byler, D.J. Safarik, K.J. McClellan, Thermophysical properties of U_3Si_2 to 1773 K, J. Nucl. Mater. 464 (2015) 275–280.
[4] D.J. Antonio, K. Shrestha, J.M. Harp, C.A. Adkins, Y. Zhang, J. Carmack, K. Gofryk, Thermal and transport properties of U_3Si_2, J. Nucl. Mater. 508 (2018) 154–158.
[5] D.R. Costa, M. Hedberg, S.C. Middleburgh, J. Wallenius, P. Olsson, D.A. Lopes, Oxidation of UN/U_2N_3-UO_2 composites: an evaluation of UO_2 as an oxidation barrier for the nitride phases, J. Nucl. Mater. 544 (2021) 152700.
[6] E.S. Wood, J.T. White, A.T. Nelson, The effect of aluminum additions on the oxidation resistance of U_3Si_2, J. Nucl. Mater. 489 (2017) 84–90.
[7] E.S. Wood, J.T. White, C.J. Grote, A.T. Nelson, U_3Si_2 behavior in H_2O: part I, flowing steam and the effect of hydrogen, J. Nucl. Mater. 501 (2018) 404–412.
[8] B. Gong, L. Cai, P. Lei, K.E. Metzger, E.J. Lahoda, F.A. Boylan, K. Yang, J. Fay, J. Harp, J. Lian, Cr-doped U_3Si_2 composite fuels under steam corrosion, Corros. Sci. 177 (2020) 109001.
[9] E.S. Wood, C. Moczygemba, G. Robles, Z. Acosta, B. Brigham, C.J. Grote, K. Metzger, L. Cai, High temperature steam oxidation dynamics of U_3Si_2 with alloying additions: Al, Cr, and Y, J. Nucl. Mater. 533 (2020) 152072.
[10] A. Mohamad, T. Yao, B. Gong, J. Harp, A.R. Wagner, A.T. Nelson, J. Lian, Aluminum-doped U_3Si_2 composite fuels with enhanced oxidation resistance, J. Alloy. Compd. 853 (2021) 157319.
[11] A. Mohamad, B. Gong, T. Yao, A.R. Wagner, M.T. Benson, J. Lian, 3Y-TZP Toughened and oxidation-resistant U_3Si_2 composites for accident tolerant fuels, J. Nucl. Mater. 544 (2021) 152691.
[12] B. Gong, T. Yao, P. Lei, L. Cai, K.E. Metzger, E.J. Lahoda, F.A. Boylan, A. Mohamad, J. Harp, A.T. Nelson, U_3Si_2 and UO_2 composites densified by spark plasma sintering for accident-tolerant fuels, J. Nucl. Mater. 534 (2020) 152147.
[13] J.T. White, A.W. Travis, J.T. Dunwoody, A.T. Nelson, Fabrication and thermophysical property characterization of UN/U_3Si_2 composite fuel forms, J. Nucl. Mater. 495 (2017) 463–474.
[14] B. Gong, E. Kardoulaki, K. Yang, A. Broussard, D. Zhao, K. Metzger, J.T. White, M.R. Sivack, K.J. Mcclellan, E.J. Lahoda, J. Lian, UN and U_3Si_2 composites densified by spark plasma sintering for accident-tolerant fuels, Ceram. Int. (2021) In press, doi:10.1016/j.ceramint.2021.12.292.
[15] A. Mohamad, Y. Ohishi, H. Muta, K. Kurosaki, S. Yamanaka, Thermal and mechanical properties of polycrystalline U_3Si_2 synthesized by spark plasma sintering, J. Nucl. Sci. Technol. 55 (10) (2018) 1141–1150.
[16] B. Gong, T. Yao, P. Lei, J. Harp, A.T. Nelson, J. Lian, Spark plasma sintering (SPS) densified U_3Si_2 pellets: microstructure control and enhanced mechanical and oxidation properties, J. Alloy. Compd. 825 (2020) 154022.
[17] K.E. Metzger, T.W. Knight, E. Roberts, X. Huang, Determination of mechanical behavior of U_3Si_2 nuclear fuel by microindentation method, Prog. Nucl. Energy 99 (2017) 147–154.
[18] B. Gong, D. Frazer, T. Yao, P. Hosemann, M. Tonks, J. Lian, Nano-and micro-indentation testing of sintered UO_2 fuel pellets with controlled microstructure and stoichiometry, J. Nucl. Mater. 516 (2019) 169–177.
[19] U. Carvajal-Nunez, T.A. Saleh, J.T. White, B. Maiorov, A.T. Nelson, Determination of elastic properties of polycrystalline U_3Si_2 using resonant ultrasound spectroscopy, J. Nucl. Mater. 498 (2018) 438–444.
[20] B. Gong, D. Frazer, B. Shaffer, H.C. Lim, P. Hosemann, P. Peralta, Micro-cantilever beam experiments and modeling in porous polycrystalline UO_2, J. Nucl. Mater. 557 (2021) 153210.
[21] W.R. Cannon, T.G. Langdon, Creep of ceramics, J. Mater. Sci. 18 (1) (1983) 1–50.
[22] K.L. Murty, Materials Ageing and Degradation in Light Water Reactors: Mechanisms and Management, Elsevier, 2013.
[23] D. Frazer, B. Shaffer, B. Gong, P. Peralta, J. Lian, P. Hosemann, Elevated temperature nanoindentation creep study of plastically deformed and spark plasma sintered UO_2, J. Nucl. Mater. 545 (2021) 152605.
[24] W. Armstrong, W. Irvine, R. Martinson, Creep deformation of stoichiometric uranium dioxide, J. Nucl. Mater. 7 (2) (1962) 133–141.
[25] E.A.C. Mercado, High temperature compression creep of U3Si2, (Order No. 10787828, University of South Carolina). *ProQuest Dissertations and Theses,* 113, University of South Carolina, 2018, Retrieved from https://www.proquest.com/docview/2071335974.
[26] K.E. Metzger, Analysis of pellet cladding interaction and creep of U3Si2 fuel for use in light water reactors, (Order No. 10165125, University of South Carolina), *ProQuest Dissertations and Theses*, 269, 2016, Retrieved from https://www.proquest.com/docview/1845027792.
[27] J.M. Harp, P.A. Lessing, R.E. Hoggan, Uranium silicide pellet fabrication by powder metallurgy for accident tolerant fuel evaluation and irradiation, J. Nucl. Mater. 466 (2015) 728–738.
[28] B. Gong, T. Yao, C. Lu, P. Xu, E. Lahoda, J. Lian, Consolidation of commercial-size UO_2 fuel pellets using spark plasma sintering and microstructure/microchemical analysis, MRS Commun. 8 (3) (2018) 979–987.
[29] F.B. Sweidan, D.H. Kim, H.J. Ryu, Minimization of the sample temperature deviation and the effect of current during high-temperature compressive creep testing by the spark plasma sintering apparatus, Materialia 9 (2020) 100550.
[30] R. Liu, W. Zhou, J. Cai, Multiphysics modeling of accident tolerant fuel-cladding U_3Si_2-FeCrAl performance in a light water reactor, Nucl. Eng. Des. 330 (2018) 106–116.
[31] M. Ugajin, M. Akabori, A. Itoh, Development of high uranium-density fuels for use in research reactors, (No JAERI-CONF–96-006) (1996).

[32] R.T. Sweet, Y. Yang, K.A. Terrani, B.D. Wirth, A.T. Nelson, Performance of U_3Si_2 in an LWR following a cladding breach during normal operation, J. Nucl. Mater. 539 (2020) 152263.
[33] Y. He, P. Chen, Y. Wu, G. Su, W. Tian, S. Qiu, Preliminary evaluation of U_3Si_2-FeCrAl fuel performance in light water reactors through a multi-physics coupled way, Nucl. Eng. Des, 328 (2018) 27–35.
[34] W. Li, K. Shirvan, U_3Si_2-SiC fuel performance analysis in BISON during normal operation, Ann. Nucl. Energy 132 (2019) 34–45.
[35] X. Chen, Y. Qin, D. Shi, Y. Guo, M. Bu, T. Yan, J. Song, G. Liu, Y. Zhang, S. Du, First-principles investigations on the anisotropic elasticity and thermodynamic properties of U_3Si_2–Al, RSC Adv. 10 (58) (2020) 35049–35056.
[36] K. Naumenko, H. Altenbach, Modeling of Creep for Structural Analysis, Springer Science & Business Media, 2007.
[37] MIT. https://abaqus-docs.mit.edu/2017/English/SIMACAEKEYRefMap/simakey-r-visco.htm.
[38] B. Ratzker, M. Sokol, S. Kalabukhov, N. Frage, Using a spark plasma sintering apparatus as a tool in a compressive creep study of fine-grained alumina, Ceram. Int. 43 (12) (2017) 9369–9376.
[39] J.P. Poirier, Creep of Crystals: High-Temperature Deformation Processes in Metals, Ceramics and Minerals, Cambridge University Press, 1985.
[40] Z. Chu, J. Yu, X. Sun, H. Guan, Z. Hu, High-temperature creep deformation and fracture behavior of a directionally solidified Ni-base superalloy DZ951, Metall. Mater. Trans. A 40 (12) (2009) 2927.
[41] K.R. Athul, U.T.S. Pillai, A. Srinivasan, B.C. Pai, A review of different creep mechanisms in Mg alloys based on stress exponent and activation energy, Adv. Eng. Mater. 18 (5) (2016) 770–794.
[42] T. Shrestha, M. Basirat, I. Charit, G.P. Potirniche, K.K. Rink, U. Sahaym, Creep deformation mechanisms in modified 9Cr–1Mo steel, J. Nucl. Mater. 423 (1–3) (2012) 110–119.
[43] A. Chokshi, T. Langdon, Characteristics of creep deformation in ceramics, Mater. Sci. Technol. 7 (7) (1991) 577–584.
[44] J.A. Yingling, Bison simulation-based identification of important design criteria for U3Si2 fuels with composite-monolithic duplex sic cladding, (Order No. 27548910, University of South Carolina), *ProQuest Dissertations and Theses*, 120, 2019, Retrieved from https://www.proquest.com/docview/2382044267.
[45] D.M. Owen, T.G. Langdon, Low stress creep behavior: an examination of Nabarro—Herring and Harper—Dorn creep, Mater. Sci. Eng. A 216 (1–2) (1996) 20–29.
[46] J. Yingling, K. Gamble, E. Roberts, R.A. Freeman, T.W. Knight, UPDATED U_3SI_2 thermal creep model and sensitivity analysis of the U_3SI_2-SIC accident tolerant FUEL, J. Nucl. Mater. 543 (2021) 152586.
[47] J. Pelleg, in: Creep in Ceramics, Springer, 2017, pp. 41–61. Creep in Ceramics.